Spectroscopic and Computational Studies of Cobalamin Species with Variable Lower Axial Ligation: Implications for the Mechanism of Co−C Bond Activation by Class I Cobalamin-Dependent Isomerases

Karen S. Conrad,[†,⊥] Christopher D. Jordan,[†] Kenneth L. Brown,[§] and Thomas C. Brunold*,[†]

[†]Department of Chemistry, University of Wisconsin-Madison, Madison, Wisconsin 53706, United States
[§]Department of Chemistry and Biochemistry, Ohio University, Athens, Ohio 45701, United States

Ⓢ Supporting Information

ABSTRACT: 5′-deoxyadenosylcobalamin (coenzyme B_{12}, AdoCbl) serves as the cofactor for several enzymes that play important roles in fermentation and catabolism. All of these enzymes initiate catalysis by promoting homolytic cleavage of the cofactor's Co−C bond in response to substrate binding to their active sites. Despite considerable research efforts, the role of the lower axial ligand in facilitating Co−C bond homolysis remains incompletely understood. In the present study, we characterized several derivatives of AdoCbl and its one-electron reduced form, Co(II)Cbl, by using electronic absorption and magnetic circular dichroism spectroscopies. To complement our experimental data, we performed computations on these species, as well as additional Co(II)Cbl analogues. The geometries of all species investigated were optimized using a quantum mechanics/molecular mechanics method, and the optimized geometries were used to compute absorption spectra with time-dependent density functional theory. Collectively, our results indicate that a reduction in the basicity of the lower axial ligand causes changes to the cofactor's electronic structure in the Co(II) state that replicate the effects seen upon binding of Co(II)Cbl to Class I isomerases, which replace the lower axial dimethylbenzimidazole ligand of AdoCbl with a protein-derived histidine (His) residue. Such a reduction of the basicity of the His ligand in the enzyme active site may be achieved through proton uptake by the catalytic triad of conserved residues, DXHXGXK, during Co−C bond homolysis.
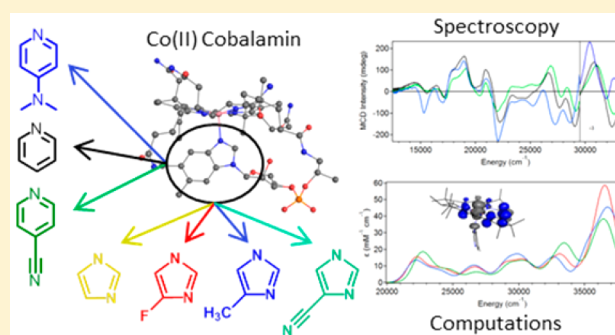
1. INTRODUCTION

5′-deoxyadenosylcobalamin (coenzyme B_{12}, AdoCbl) has attracted extensive scientific interest due to its complex structure and biological role in initiating rearrangement reactions that proceed via a radical mechanism.[1−3] AdoCbl-dependent enzymes play important roles in fermentation and catabolism[4,5] and are found mostly in bacteria. In humans, the only enzyme requiring AdoCbl for activity is methylmalonyl-CoA mutase (MMCM).[6] AdoCbl consists of a six-coordinate, low-spin Co(III) ion ligated equatorially by four nitrogens of a tetrapyrrollic corrin macrocycle and coordinated axially by a 5′-deoxyadenosyl group in the upper (β) position and a dimethylbenzimidazole base (DMB) in the lower (α) position (Figure 1). The DMB base is also covalently bound to a side chain of the corrin ring through a nucleotide loop. In biological systems, the radical reactions involving AdoCbl are initiated by enzyme-induced homolytic cleavage of the cofactor's Co−C bond. The rate by which AdoCbl-dependent enzymes accelerate Co−C bond homolysis is remarkable (∼12 orders of magnitude, corresponding to a lowering of the bond dissociation energy by ∼17 kcal/mol).[7,8] The products of this homolysis reaction are a five-coordinate Co(II)Cbl species and an adenosyl radical (Ado•). The Ado• radical abstracts a

hydrogen atom from the substrate molecule to form 5′-deoxyadenosine and a substrate-based radical. Rearrangement of this radical species, followed by reabstraction of the hydrogen from adenosine, leads to the formation of product. Once the product is released, Ado• and Co(II)Cbl combine to regenerate AdoCbl and close the catalytic cycle.

Two classes of AdoCbl-dependent isomerases exist that differ with respect to the mode by which the cofactor binds to the enzyme active site. Class I isomerases,[1] which include MMCM, replace the lower axial DMB ligand with a protein-derived histidine (His) residue, so as to bind the cofactor in a "His-on" manner. This coordinating histidine participates in a hydrogen-bonding network as part of a conserved DXHXGXK sequence.[9,10] (In one class I enzyme, 2-methyleneglutarate mutase, the AdoCbl-binding sequence is DXHXGXN.)[11] Alternatively, Class II eliminases[2,12] retain the axial DMB coordination upon incorporation of the cofactor into the enzyme active site, thus binding it in a "DMB-on" fashion.

While cofactor analogues with modified lower axial ligands can retain most of their activity in Class I enzymes,[13,14] even
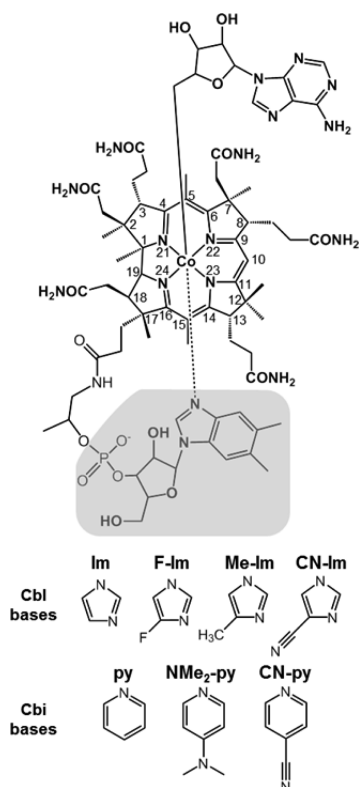
Figure 1. Structure of AdoCbl and α-axial ligands used in this study. Note that in cobinamides, the shaded region including the nucleotide loop and native DMB ligand are missing. The coordinating nitrogen in the imidazole bases is proximate to the substituent.

when they do not exhibit His coordination,[15] replacement of the coordinating His side chain[16−18] or its hydrogen bonding partners[16,17] causes a dramatic loss in activity. Despite this evidence for the importance of the lower axial ligand environment, most experimental investigations[19−24] of B_{12}-dependent isomerases have focused on the interaction between the protein, its substrate, and the cofactor's upper axial ligand. Thus, the means by which the coordinating His residue and its conserved hydrogen bonding partners contribute to catalysis have not yet been determined.

In principle, enzymatic activation of the cofactor's Co−C bond may be achieved via a combination of two fundamentally different mechanisms. In one mechanism,[25,26] the protein activates this bond by destabilizing the six-coordinate AdoCbl reactant state by imposing geometric and/or electronic constraints within the active site. Alternatively, in the other mechanism,[27] the enzyme stabilizes the five-coordinate Co(II)-Cbl and Ado$^{\bullet}$ posthomolysis products through favorable hydrogen bonding and/or electrostatic interactions within the active site. While both mechanisms may contribute to a lowering of the Co−C bond homolysis barrier, the importance of the latter mechanism is supported by previous spectroscopic and computational investigations from our laboratory[28,29] and several other studies,[20,23,30−32] including recent computational work on MMCM.[33]

Spectroscopic studies of the glutamate mutase (GM)[29] and MMCM[28,34] Class I enzymes have led to the proposal that the posthomolysis product stabilization is achieved, in part, by a relatively uniform stabilization of the Co 3d-based molecular orbitals (MOs) of Co(II)Cbl bound to these proteins. This stabilization was particularly apparent in the corresponding

magnetic circular dichroism (MCD) spectra, which showed that binding of Co(II)Cbl to GM and MMCM induced noticeable blue-shifts of features in a region of the spectrum that is dominated by metal-to-ligand charge transfer (MLCT) transitions, while the ligand field (LF) and corrin-based $\pi \rightarrow \pi^*$ transitions displayed negligible shifts. Alternatively, the MCD spectra of free and GM- or MMCM-bound AdoCbl were found to be nearly identical, indicating that enzyme-induced perturbations to the electronic structure of AdoCbl are relatively minor.[29,34]

The means by which the Co 3d-based MOs of enzyme-bound Co(II)Cbl are tuned by Class I isomerases, and to what extent the α-axial ligand contributes to this tuning, remains an open question. One possibility is the coupling of the Co−C bond homolysis step to proton uptake by the His, Asp, Lys triad in the conserved DXHXGXK motif that provides the α-axial His ligand in both MMCM and GM.[35] Coupling of Co−C bond homolysis to proton uptake would reduce charge donation from the axial His ligand to the cobalt ion in enzyme-bound Co(II)Cbl, thus stabilizing this state. Such a mechanism is reminiscent of Pratt's "molecular switch" postulate, which theorized that changes in protein conforma-tion—or, in this case, protonation—could thermodynamically favor certain states.[36,37] To evaluate the effect of reducing the donor strength of the α-axial ligand on the rate of Co−C bond homolysis, Brown and co-workers prepared a unique analogue of AdoCbl, adenosyl(5-fluoroimidazole)cobalamin [Ado(F-Im)Cbl], that possesses a 5-fluoroimidazole in the α-axial position. They found that when the Ado(F-Im)Cbl analogue was used as a cofactor in ribonucleoside triphosphate reductase (RNTR), which binds AdoCbl in the DMB-on form, k_{obs} dropped ~65-fold from the value obtained with adenosyl-(imidazole)cobalamin (AdoImCbl) and over 300-fold from that of the native (i.e., AdoCbl-bound) enzyme.[38] This reduction in catalytic efficiency led to the suggestion that the low basicity of F-Im[39] (pK_b = 11.6) relative to that of Im[40] (pK_b = 7.2) is responsible for the enhanced stability of the Co−C bond in RNTR-bound Ado(F-Im)Cbl.[41]

Previous computational studies have established a weak dependence of the Co−C bond dissociation energy on the basicity of the trans α-axial base.[42] The question of whether the Co−N$_{ax}$ bond length correlates with the energy required for the homolytic cleavage of the Co−C bond was initially raised when hyper-long Co−N$_{ax}$ bonds were observed in the X-ray crystal structures of MMCM-bound AdoCbl[43] and subsequent EXAFS spectroscopic studies.[44] However, computations have revealed that the length of the Co−N$_{ax}$ bond has only minor effects on the energy required for Co−C bond homolysis; thus, elongation of the Co−N$_{ax}$ bond alone cannot account for the extent of enzymatic activation.[45] Nevertheless, the unique nature of the C−Co−N$_{ax}$ axial bonding scheme, with its competing σ and π effects, has continued to be the subject of a variety of computational,[46−49] kinetic,[50] and spectroscopic[51,52] studies.

In the present study, we characterized Ado(F-Im)Cbl and its one-electron reduced form Co(II)(F-Im)Cbl by using elec-tronic absorption (Abs) and magnetic circular dichroism (MCD) spectroscopies. To complement our experimental data, we performed computations on these species, as well as the reduced forms of three other cobalamin analogues: Co(II)(imidazole)cobalamin [Co(II)ImCbl], Co(II)(5-cyanoimidazole)cobalamin [Co(II)(CN-Im)Cbl], and Co(II)-(5-methylimidazole)cobalamin [Co(II)(Me-Im)Cbl]. Addition-

al spectroscopic and computational studies were performed on a series of Co(II) cobinamide [Co(II)Cbi⁺] species, which lack the native cofactor's nucleotide loop and DMB (Figure 1). Cobinamides with axial ligation from pyridine (py), 4-cyanopyridine (CN-py), and 4-(dimethylamino)-pyridine (Me₂N-py) were investigated. The geometries of all Cbl and Cbi species were optimized using a quantum mechanics/molecular mechanics (QM/MM) method, and the optimized geometries were used to compute Abs spectra with time-dependent density functional theory (TD-DFT). Collectively, our spectroscopic and computational results indicate that a reduction in the basicity of the lower axial ligand induces changes to the cofactor's electronic structure in the reduced state similar to those observed upon binding of Co(II)Cbl to Class I isomerases.

2. EXPERIMENTAL AND COMPUTATIONAL METHODS

2.1. Cofactor Analogue Syntheses. Ado(5-F-Im)Cbl was synthesized using a "guided biosynthesis" in which the fermentation of *Propionibacterium shermanii* on media supplemented with 4(5)-fluoroimidazole produced CN(5-F-Im)Cbl and CN(4-F-Im)Cbl. Subsequent separation and adenosylation of the CN(5-F-Im)Cbl derivative to form Ado(5-F-Im)Cbl was completed according to previously published procedures, and the product was characterized as described in the literature.[38,53−56]

All pyridine bases, (py, CN-py, and Me₂N-py), dicyanocobinamide [(CN)₂Cbi], methanol, and sodium borohydride (NaBH₄) were purchased from Sigma-Aldrich and used as obtained. Diaquocobinamide [(H₂O)₂Cbi²⁺] was prepared as described previously, by reducing (CN)₂Cbi with NaBH₄ and loading the reaction mixture on a C18 SepPack column, washing with doubly distilled H₂O, and eluting the product with methanol.[57,58] Co(II)Cbi⁺ was prepared by the addition of NaBH₄ to a degassed solution of (H₂O)₂Cbi²⁺ containing 60% (v/v) glycerol. The pyridine solutions also contained 60% (v/v) glycerol and were degassed before adding an approximately threefold molar excess to the Co(II)Cbi⁺ solution. The conversion of Co(II)Cbi⁺ to pyridylcobinamide [Co(II)pyCbi⁺] was monitored spectrophotometrically. The syntheses of 4-cyanopyridylcobinamide [Co(II)(CN-py)Cbi⁺] and 4-dimethylaminopyridylcobinamide [Co-(II)(Me₂N-py)Cbi⁺] were accomplished by the same procedure using the appropriate pyridine derivative. The identities of these compounds were confirmed by electron paramagnetic resonance (EPR) spectroscopy (Supporting Information, Figure S1 and Table S1).[59]

2.2. Spectroscopy. Low-temperature Abs and MCD spectra were obtained using a Jasco J-715 spectropolarimeter in conjunction with an Oxford Instruments SM-4000 8 T magnetocryostat. All MCD spectra reported herein were obtained by taking the difference between spectra collected with the magnetic field aligned parallel and antiparallel to the light propagation axis to eliminate contributions from the natural CD and glass strain. X-Band EPR spectra were obtained using a Bruker ESP 300E spectrometer equipped with an Oxford ESR 900 continuous-flow liquid helium cryostat and an Oxford ITC4 temperature controller, and a Varian EIP model 625A frequency counter. In each case a modulation frequency of 100 kHz was used, along with a modulation amplitude of 10.456 G, and a time constant of 40.96 ms. EPR spectral fits to obtain *g* and *A* values were completed using the WEPR program developed by Dr. Frank Neese.[60]

2.3. Computational Methods. All computational models were generated from the highest-resolution X-ray crystal structure of AdoCbl (CCDC file: DADCBL).[61] Initial geometries for Co(II)Cbl and all cofactor analogues included in this study were constructed from this structure by adding or removing the necessary atoms in silico. A geometry optimization of each model was performed with the ONIOM QM/MM method[62] as implemented in Gaussian 09.[63] The QM region for all models consisted of the Co ion, the corrin macrocycle, including the first carbon of each of its side chains, the complete lower axial ligand, and, in the adenosylated models, the ribose moiety of the upper axial ligand. The MM region consisted of

the remainder of the upper axial ligand (when present) and the remainder of all corrin side chains. All covalent bonds spanning the QM/MM boundary were capped with hydrogen atoms (i.e., link atoms) during the QM steps of the optimization. The new X−H bond lengths were set equal to the original bond length scaled by 0.709. The QM region was treated with the BP86 density functional,[64,65] which is known to be well-suited for obtaining realistic geometries of cobalamins.[66] The spin-unrestricted formalism was used for all Co(II) models. The triple-ζ basis set with an additional polarization function (TZVP) developed by Ahlrichs[67] was used for the Co ion and all coordinating N and C atoms, while the split-valence polarized (SVP) basis set from the same group[68] was used for all other atoms. The MM region was modeled with the force field specifically developed for cobalamins by Marques et al.[69] The default ONIOM convergence criteria for SCF cycles and geometry optimizations were used.

TD-DFT was used to compute Abs spectra for the QM regions of all optimized models. The scheme for capping the QM region with hydrogen atoms was the same as in the geometry optimizations described above. All MM atoms aside from those explicitly replaced with H atoms were included in the computations as point charges with values defined by the force field used in the QM/MM optimization. The 60 lowest-energy transitions involving MOs within ±4 hartree of the highest occupied molecular orbital−lowest unoccupied molecular orbital (HOMO−LUMO) gap were computed by employing the B3LYP density functional[64,70] and the same basis sets as in the geometry optimizations. While B3LYP is known to poorly predict some cobalamin properties, such as Co−C bond dissociation energies, we have used it successfully in the past to compute Abs spectra of cobalamin species in both the Co(III) and Co(II) oxidation states.[28,71,72] Additionally, it has been noted that the Abs spectra of Cbl species predicted by BP86 and B3LYP display negligible differences.[73] Nevertheless, additional DFT and TD-DFT computations were performed using the TPSSh hybrid functional[74] to ensure that our findings were not biased by the computational method used (see Figures S5−S7 of the Supporting Information). All TD-DFT computations were performed with the Orca 2.9.1 program[75] and used the resolution of the identity[76] and Tamm-Dancoff approximations[77] to speed the calculations. Simulated Abs spectra were generated on the basis of the TD-DFT results by using a constant bandwidth of 1500 cm⁻¹ for all transitions. All isosurface plots of MOs and electron density difference maps (EDDMs) were generated with PyMol[78] using isodensity values of 0.06 and 0.003 au, respectively.

3. RESULTS

3.1. Spectroscopic Data for AdoCbl and Ado(F-Im)Cbl. The Abs and MCD spectra of AdoCbl and Ado(F-Im)Cbl are shown in Figure 2. In general, the Abs spectra of alkylcobalamins exhibit many overlapping features that can be loosely grouped into three categories.[72] The lowest-energy features, termed the α/β bands, peak below 21 000 cm⁻¹. They were assigned as the electronic origin and vibronic sideband of the HOMO → LUMO (corrin π → π*) transition. The transitions responsible for the features at slightly higher energies (the D/E bands) also contain corrin π → π* character, along with some metal-to-ligand charge transfer (MLCT) character. The dominant features above 26 000 cm⁻¹ are collectively referred to as the γ bands, which arise from energetically proximate transitions involving primarily corrin π → π* excitation. The same sets of transitions also produce the major features in the MCD spectrum. However, because the MCD signal is a signed quantity and the intensity is governed by different selection rules than the Abs intensity, MCD spectroscopy provides a much better probe of the number of transitions contributing to a given spectral region. A previous spectroscopic and computational investigation of methylcobalamin, another biologically relevant Co(III)Cbl species whose Abs and MCD spectra are nearly indistinguishable from those
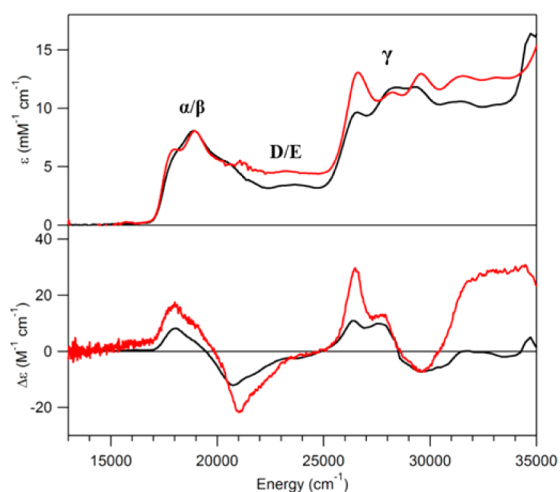
Figure 2. Abs and 7 T MCD spectra obtained at 4.5 K of AdoCbl (black) and Ado(F-Im)Cbl (red).

of AdoCbl, revealed that the γ bands have contributions from at least seven distinct electronic transitions with varying degrees of corrin-$\pi \rightarrow \pi^*$, MLCT, and ligand-to-metal charge transfer (LMCT) character.[72] As a result, this spectral region is particularly sensitive to axial ligand substitutions, as demonstrated in a recent spectroscopic and computational investigation of a series of Co(III)Cbl and Co(III)Cbi$^+$ species.[79]

Despite the difference in lower axial ligand basicity, AdoCbl and Ado(F-Im)Cbl exhibit similar electronic Abs spectra. Likewise, the MCD spectra of these species are qualitatively similar, although the negative feature at 20 700 cm^{-1} in the AdoCbl spectrum is blue-shifted by ~300 cm^{-1} in the Ado(F-Im)Cbl spectrum. Moreover, a significant redistribution of the intensities and small changes in the positions of the γ bands are observed in both the Abs and MCD spectra. Although these changes are small in magnitude, they are more significant than those induced by the binding of AdoCbl to the Class I isomerases MMCM and GM.[29,34]

3.2. Computational Data for AdoCbl and Ado(F-Im)Cbl. The geometry optimizations of complete AdoCbl and Ado(F-Im)Cbl models resulted in cofactor structures with small but noticeable differences (Supporting Information, Figure S2). While the sterically bulky DMB ligand of AdoCbl has little conformational flexibility, the smaller F-Im ligand rotates around the Co—N$_{ax}$ bond, as indicated by an opening of the C$_{10}$(cor)—Co—N$_{ax}$—C$_1$(Im/DMB) dihedral angle from 94.4° to 102.8°. This rotation induces geometric changes along the side chain that connects the lower axial ligand to the corrin ring, which causes one of the nitrogen atoms coordinated to the Co to be pushed out of the equatorial plane (Supporting Information, Table S2). Substitution of DMB with F-Im also leads to a decrease in the Co—N$_{ax}$ bond length from 2.382 to 2.328 Å. In contrast, the upper axial Co—C bond length is virtually unperturbed by the lower axial ligand switch, changing by a mere 0.001 Å from AdoCbl to Ado(F-Im)Cbl. The lack of a change in Co—C bond length is consistent with a previous theoretical investigation, which found no correlation between lower axial ligand basicity and Co—C bond length in cobinamides.[42]

The computed MO diagrams for AdoCbl and Ado(F-Im)Cbl are shown in Figure 3. The main differences between the two are the relative energies of the MOs containing contributions from the lower axial ligand. Although the heavily mixed

compositions of the MOs make direct comparisons difficult, we note that in Ado(F-Im)Cbl the F-Im-based orbitals (e.g., MO No. 201) are considerably lower in energy than the nonbonding Co 3d$_{xy}$-based orbital (MO No. 204). Thus, the MOs derived from the frontier orbitals of the F-Im ligand contain little contributions from the Co 3d manifold and corrin ring orbitals. On the other hand, the DMB-derived MOs of AdoCbl are higher in energy than the Co 3d$_{xy}$-based orbital (MO Nos. 221 and 222 versus MO No. 216), and thus contain large orbital contributions from the rest of the cofactor.

The TD-DFT computed Abs spectra for AdoCbl and Ado(F-Im)Cbl are shown in Figure 4, and details regarding key transitions are provided in Tables 1 and 2. The spectra are very similar in the α/β and D/E regions aside from a slightly smaller splitting between the two regions in the Ado(F-Im)Cbl spectrum. The lower ligand substitution does, however, give rise to a major rearrangement of intensity in the γ region. Although the close energetic proximity of numerous transitions with similar character make a qualitative analysis of this region difficult, one important observation is the appearance of a new feature ~1000 cm^{-1} lower in energy than the onset of the γ region in the Ado(F-Im)Cbl spectrum. This feature is due to transition 5, which mainly entails HOMO (corrin π) $\rightarrow$ LUMO +2 (Co 3d$_{x^2-y^2}$) excitation. The corresponding transition in the AdoCbl spectrum occurs at much higher energy because of the larger destabilization of the Co 3d$_{x^2-y^2}$-based orbital (MO No. 230, Supporting Information, Figure S3). The relative stabilization of the Co 3d$_{x^2-y^2}$-based orbital in Ado(F-Im)Cbl (MO No. 210) is unlikely to be a direct consequence of the lower axial ligand switch, but may be a result of the increased folding of the corrin ring in the Ado(F-Im) model, which mitigates the σ^* antibonding interaction between the Co 3d$_{x^2-y^2}$ orbital and the "lone pairs" on the four coordinating nitrogens of the corrin ring. While the experimental Abs spectrum of Ado(F-Im)Cbl seemingly lacks the new feature observed in the computed spectrum, shifts of one or more of the transitions contributing to the γ bands could be responsible for the intensity redistribution in this region. As such, the experimental and computed Abs spectra agree on there being small changes in the α/β and D/E regions, and more significant perturbations to the γ bands when the DMB ligand of AdoCbl is replaced with F-Im.

3.3. Spectroscopic Data for Co(II)Cbl and Co(II)-Bound Derivatives. The Abs and MCD spectra of Co(II)Cbl and Co(II)(F-Im)Cbl are presented in Figure 5. The Co(II)Cbl Abs and MCD spectra have previously been analyzed by our laboratory,[71] which led to the following general band assignments. The lowest energy features (<17 000 cm^{-1}) are due to LF transitions. These formally parity-forbidden transitions carry negligible intensity in the Abs spectrum, but gain intensity in the MCD spectrum through spin–orbit coupling. All features above 17 000 cm^{-1} arise from transitions involving a combination of MLCT and corrin $\pi \rightarrow \pi^*$ one-electron excitations. The former dominate for transitions between 17 000 and 20 500 cm^{-1}, while the latter are the main contributors to the intense transitions at higher energies.

Visual inspection of the Co(II)Cbl and Co(II)(F-Im)Cbl Abs and MCD spectra reveals small variations in the intensities and positions of certain features. To quantify these changes, we performed iterative Gaussian deconvolutions of the Abs and MCD spectra using the lowest acceptable number of individual transitions required to fit the experimental data (Supporting Information, Figure S4, Tables S2 and S3). Of the 18
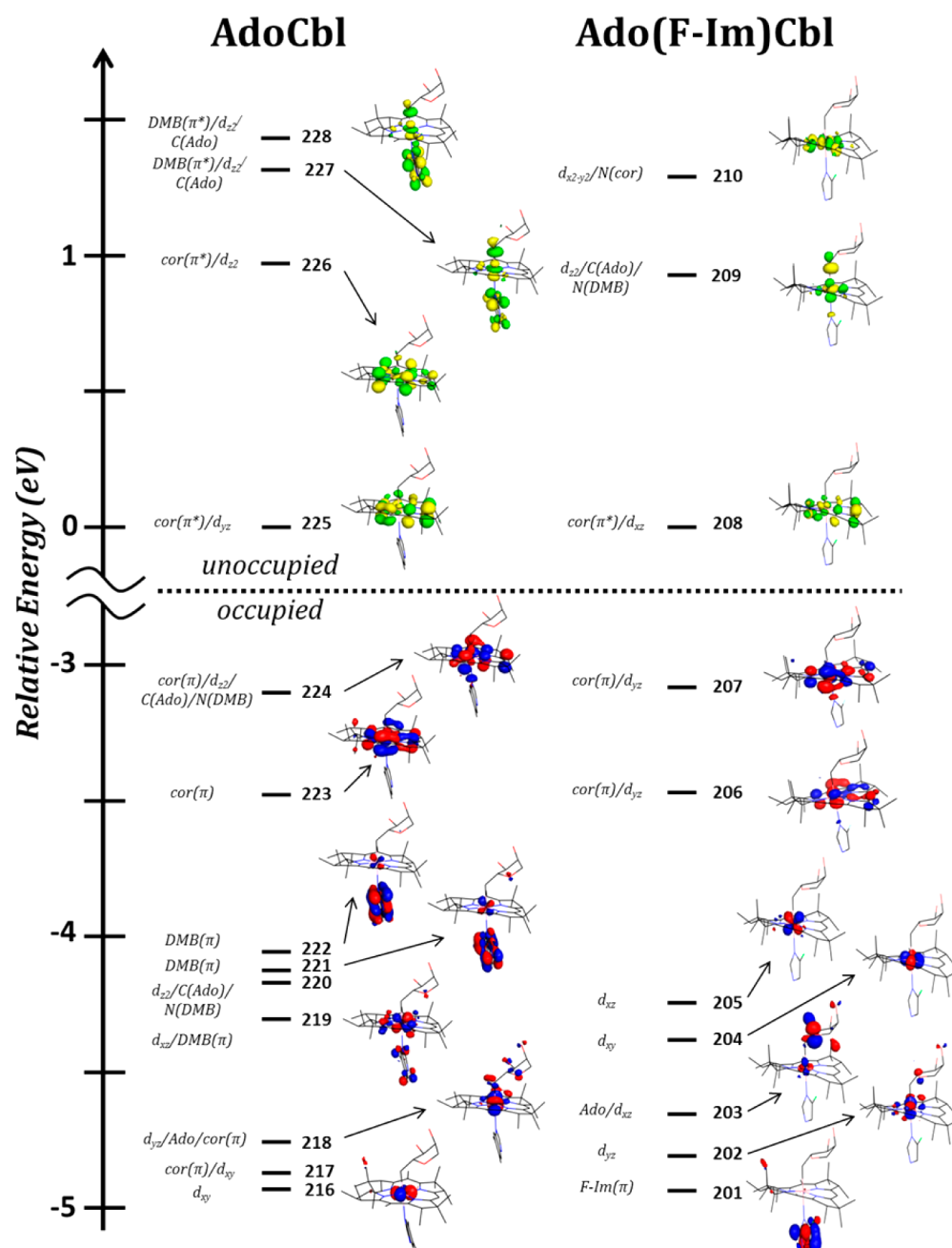
Figure 3. DFT-computed MO diagrams for AdoCbl and Ado(F-Im)Cbl. MOs were shifted vertically to align the LUMOs at 0 eV. Occupied orbitals are shown in red and blue; unoccupied orbitals are shown in green and yellow.

transitions in the Co(II)Cbl spectrum below 35 000 cm^{-1} identified in this analysis, 11 exhibit blue-shifts of 100 cm^{-1} or more upon switching the lower axial ligand to F-Im (Table 3). These 11 transitions are all centered above 16 000 cm^{-1}, indicating they have predominantly MLCT or corrin $\pi \rightarrow \pi^*$ character. The origin of these blue-shifts is explored computationally in Section 3.4.

To further investigate the influence of the α-axial ligand basicity on the electronic spectra of Co(II)Cbl analogues, we also performed spectroscopic studies of Co(II)pyCbi$^+$, Co(II)-(CN-py)Cbi$^+$, and Co(II)(Me$_2$N-py)Cbi$^+$. The MCD spectra of these three species (Figure 6) are very similar to those obtained for Co(II)Cbl and Co(II)(F-Im)Cbl (Figure 5), also exhibiting low energy LF transitions and higher energy MLCT and corrin $\pi \rightarrow \pi^*$ transitions. Inspection of these spectra

reveals that an increased basicity of the lower axial ligand is correlated with a general red-shift of Abs and MCD features. Specifically, the Co(II)(Me$_2$N-py)Cbi$^+$ (pK_b of Me$_2$N-py = 4.3) spectrum is red-shifted relative to the Co(II)pyCbi$^+$ (pK_b of py = 8.7) spectrum, which in turn is red-shifted from that of Co(II)(CN-py)Cbi$^+$ (pK_b of CN-py = 12.1). As in the case of the Co(II)Cbl and Co(II)(F-Im)Cbl spectra, the largest shifts involve features at intermediate and high energies (above 17 000 cm^{-1}).

3.4. Computational Data for Co(II)Cbl and Co(II)-Bound Derivatives. To identify the electronic structural origin of the differences in the Abs and MCD spectra of Co(II)Cbl and Co(II)(F-Im)Cbl, and to explore how the basicity of the lower axial ligand is linked to these differences, we computed equilibrium geometries and Abs spectra for
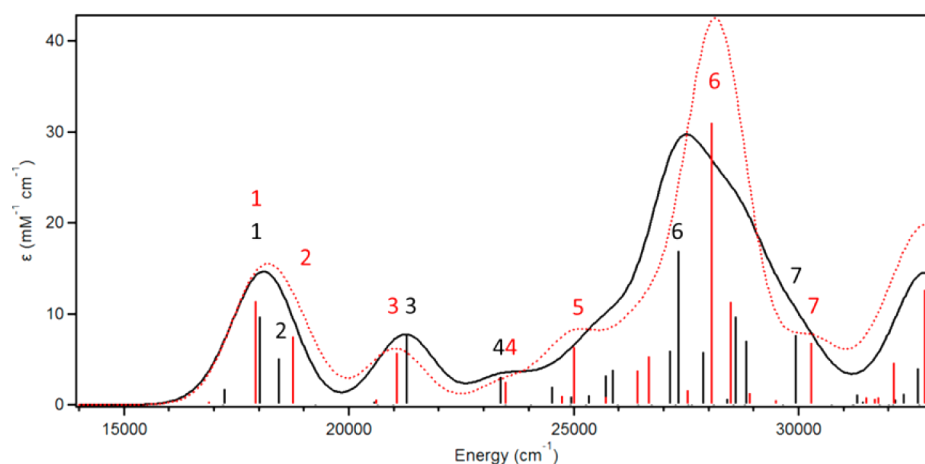
Figure 4. TD-DFT computed Abs spectra for AdoCbl (black, solid) and Ado(F-Im)Cbl (red, dashed). A uniform red-shift of 3000 cm^{-1} was applied to facilitate a comparison with the experimental spectra in Figure 2. The computed energies and intensities of individual transitions are shown as sticks. Details regarding the labeled transitions are provided in Tables 1 and 2

Table 1. TD-DFT Computed Energies, Oscillator Strengths, and Percent Contributions from Dominant One-Electron Excitations for the Major Electronic Transitions of AdoCbl

state	E (cm^{-1})	f	transition	%	donor MO	acceptor MO
1	18 014	0.066 89	224 → 225	53	corrin π/Co 3d$_{z^2}$/C(Ado)/N(DMB)	corrin π*/Co 3d$_{yz}$
2	18 445	0.0350	224 → 225	20	corrin π/Co 3d$_{z^2}$/C(Ado)/N(DMB)	corrin π*/Co 3d$_{yz}$
			219 → 227	10	Co 3d$_{xz}$/DMB-π	DMB-π*/Co 3 d$_{z^2}$/C(Ado)
3	21 279	0.0524	223 → 225	64	corrin π	corrin π*/Co 3d$_{yz}$
			224 → 226	22	corrin π/Co 3d$_{z^2}$/C(Ado)/N(DMB)	corrin π*/Co 3d$_{z^2}$
4	23 367	0.0208	219 → 225	28	Co 3d$_{xz}$/DMB-π	corrin π*/Co 3d$_{yz}$
			222 → 225	22	DMB-π	corrin π*/Co 3d$_{yz}$
			221 → 225	22	DMB-π	corrin π*/Co 3d$_{yz}$
6	27 327	0.1170	224 → 226	30	corrin π/Co 3d$_{z^2}$/C(Ado)/N(DMB)	corrin π*/Co 3d$_{z^2}$
			223 → 226	15	corrin π	corrin π*/Co 3d$_{z^2}$
7	29 939	0.0530	218 → 225	42	Co 3d$_{yz}$/Ado/corrin π	corrin π*/Co 3d$_{yz}$
			216 → 225	18	Co 3d$_{xy}$	corrin π*/Co 3d$_{yz}$

Table 2. TD-DFT Computed Energies, Shifts from Corresponding AdoCbl Transitions, Oscillator Strengths, and Percent Contributions from Dominant One-Electron Excitations for the Major Electronic Transitions of Ado(F-Im)Cbl

state	E (cm^{-1})	shift (cm^{-1})	f	transition	%	donor MO	acceptor MO
1	17 927	−87	0.0787	207 → 208	61	corrin π/Co 3d$_{yz}$	corrin π*/Co 3d$_{xz}$
2	18 760	315	0.0516	207 → 208	24	corrin π/Co 3d$_{yz}$	corrin π*/Co 3d$_{xz}$
				205 → 210	17	Co 3d$_{xz}$	Co 3d$_{x^2-y^2}$/N(cor)
3	21 073	−206	0.0395	206 → 208	61	corrin π/Co 3d$_{yz}$	corrin π*/Co 3d$_{xz}$
				207 → 209	29	corrin π/Co 3d$_{yz}$	Co 3d$_{z^2}$/C(Ado)/N(F-Im)
4	23 491	124	0.0174	205 → 208	67	Co 3d$_{xz}$	corrin π*/Co 3d$_{xz}$
5	25 008		0.0437	207 → 210	60	corrin π/Co 3d$_{yz}$	Co 3d$_{x^2-y^2}$/N(cor)
6	28 062	735	0.2145	207 → 209	26	corrin π/Co 3d$_{yz}$	Co 3d$_{z^2}$/C(Ado)/N(F-Im)
				207 → 210	15	corrin π/Co 3d$_{yz}$	Co 3d$_{x^2-y^2}$/N(cor)
7	30 287	348	0.0469	200 → 208	38	Ado	corrin π*/Co 3d$_{xz}$
				202 → 208	28	Co 3d$_{yz}$	corrin π*/Co 3d$_{xz}$

Co(II)Cbl and seven Co(II)-bound derivatives. Three of these derivatives are the Cbi species with variable pyridyl bases described in the previous section, and the remaining four are Cbl species with modified bases, including the spectroscopically characterized derivative Co(II)(F-Im)Cbl, as well as Co(II)-ImCbl, Co(II)(CN-Im)Cbl, and Co(II)(Me-Im)Cbl.

The TD-DFT computed Abs spectra for Co(II)Cbl and the four Co(II)Cbl derivatives are shown in Figure 7, and a summary of the relevant results obtained for Co(II)Cbl and Co(II)(F-Im)Cbl is provided in Tables 4 and 5. (Isosurface

plots of all frontier MOs can be found in Tables S5 and S6 of the Supporting Information.) An initial comparison of the computed spectra for Co(II)Cbl and Co(II)(F-Im)Cbl reveals that many of the major features of the latter are blue-shifted relative to those of the former, as observed in the experimental MCD spectra (Table 3). This is especially apparent for the transitions with energies between 20 000 and 31 000 cm^{-1}, a range in which five of the most intense transitions are computed at higher energies in the Co(II)(F-Im) spectrum. Features in this region of the Abs and MCD spectra of
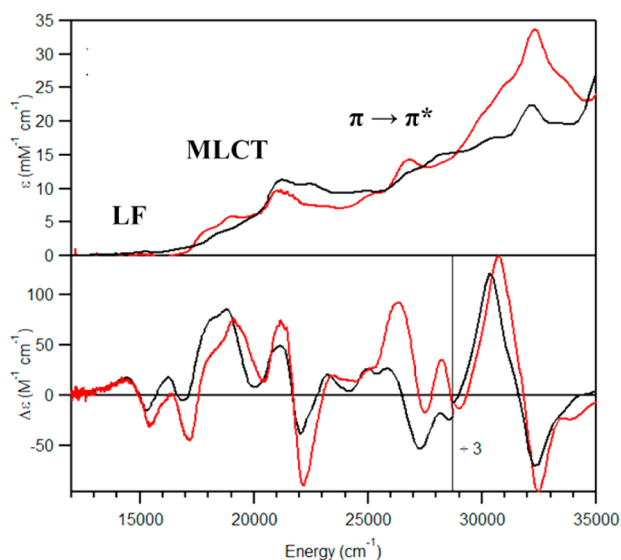
Figure 5. Abs and 7 T MCD spectra obtained at 4.5 K of Co(II)Cbl (black) and Co(II)(F-Im)Cbl (red).

Table 3. Selected Spectral Features of Co(II)(F-Im)Cbl and Shifts Relative to Co(II)Cbl Counterparts

band	energy (cm^{-1})	shift (cm^{-1})	assignment[a]
4	17 260	150	MLCT/ $\pi \to \pi^*$
5	17 900	200	MLCT/ $\pi \to \pi^*$
6	19 170	340	MLCT/ $\pi \to \pi^*$
8	21 300	250	$\pi \to \pi^*$/ MLCT
12	25 150	200	$\pi \to \pi^*$/ MLCT
13	26 390	350	$\pi \to \pi^*$/ MLCT
14	27 460	200	$\pi \to \pi^*$/ MLCT
15	28 380	380	$\pi \to \pi^*$/ MLCT
16	28 900	130	$\pi \to \pi^*$/ MLCT
17	30 650	350	$\pi \to \pi^*$/ MLCT
18	31 670	220	$\pi \to \pi^*$/ MLCT
20	32 510	−140	$\pi \to \pi^*$/ MLCT
21	34 170	−1600	$\pi \to \pi^*$/ MLCT

[a]See text for more details.

Co(II)Cbl have previously been attributed to transitions with predominant MLCT and corrin $\pi \to \pi^*$ character (vide supra). These assignments are corroborated by the computed electron

density difference maps (EDDMs) for transitions 1−5 shown in Figure 8.

A direct comparison of the TD-DFT results for Co(II)Cbl and Co(II)(F-Im)Cbl is complicated by the fact that the MOs involved in the transitions at energies >31 000 cm^{-1} have considerable contributions from the lower axial ligand, making it unclear whether the predicted spectral differences are actually due to the decreased basicity of F-Im. To address this issue, we extended our computational analysis to models of Co(II)Cbl derivatives with substituted imidazole bases more closely related to F-Im. As shown in Figure 7, all major Abs features below 35 000 cm^{-1} shift when the lower axial ligand is varied, with the lowest-energy features found in Co(II)(Im)Cbl, followed by Co(II)(Me-Im)Cbl, Co(II)(F-Im)Cbl, and Co-(II)CN-Im(Cbl). This trend reflects the electron-withdrawing power of the Im substituents, with Me < F < CN. The Co(II)ImCbl model provides an exception to this trend, as it would ordinarily be expected to have transitions between those of Co(II)(Me-Im)Cbl and Co(II)(F-Im)Cbl. This anomaly is likely a result of the much shorter Co−N$_{ax}$ bond distance in Co(II)ImCbl (2.11 Å) than in the other Co(II)Cbl models possessing substituted Im bases (2.17−2.23 Å) due, at least in part, to steric crowding with the corrin ring in the latter. Thus, even though Im is a weaker base than Me-Im,[80] the shorter bond distance in Co(II)ImCbl leads to increased charge donation from the α-axial ligand, effectively mimicking the binding of a stronger base.

The TD-DFT computed Abs spectra for the three Co(II)-Cbi$^+$ derivatives are presented in Figure 9. Consistent with our experimental data (Figure 6), transitions at energies <20 000 cm^{-1} have predominantly LF character and thus carry little Abs intensity (note that the intense feature at 17 000 cm^{-1} in the computed Co(II)(CN-py)Cbi$^+$ Abs spectrum is due to a transition with significant Co 3d → (CN-py) π^* character). As was predicted for the Co(II)-bound Cbl models, all computed transitions for the Co(II)Cbi$^+$ derivatives above 20 000 cm^{-1} contain considerable MLCT character. Most importantly, sizable blue shifts of most Abs features are predicted computationally when the basicity of the lower axial ligand is decreased (Me$_2$N-py < py < CN-py), consistent with our MCD data (Figure 6).
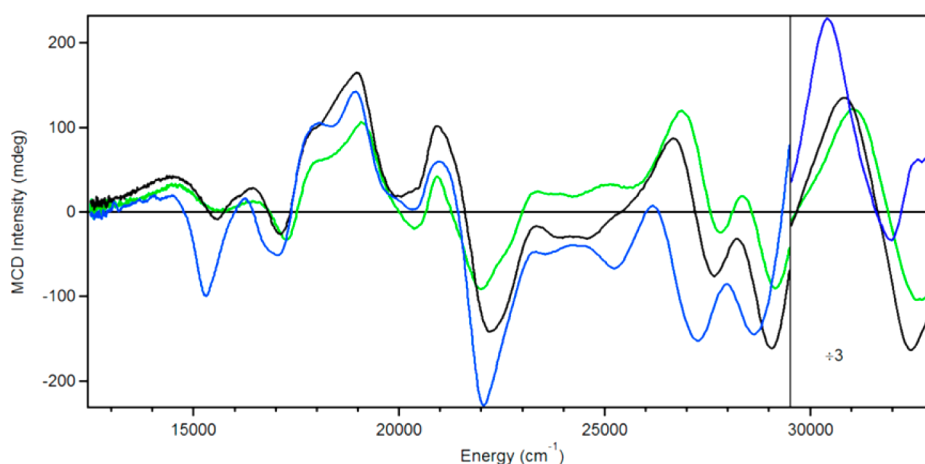
Figure 6. MCD spectra obtained at 7 T and 4.5 K of Co(II)pyCbi$^+$ (black), Co(II)(CN-py)Cbi$^+$ (green), and Co(II)(Me$_2$N-py)Cbi$^+$ (blue).
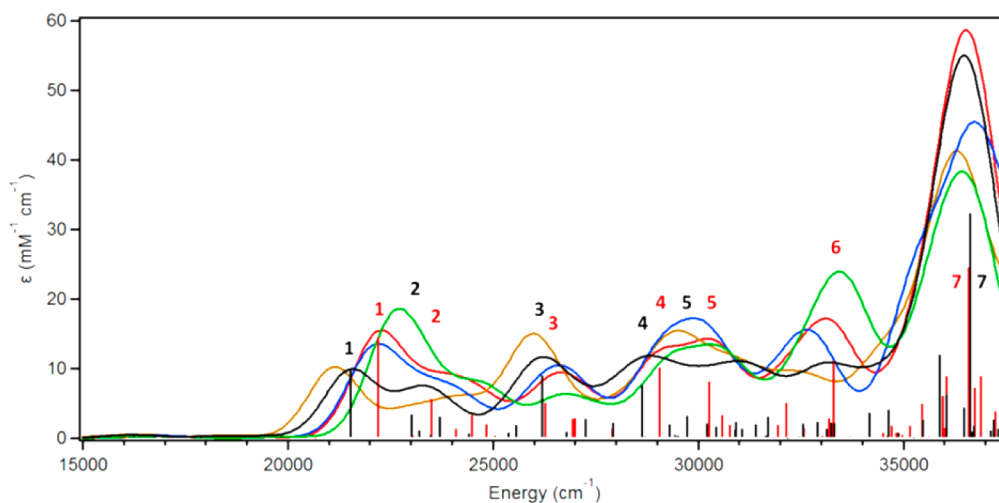
Figure 7. TD-DFT computed Abs spectra for Co(II)Cbl (black), Co(II)(F-Im)Cbl (red), Co(II)ImCbl (gold), Co(II)(Me-Im)Cbl (blue), and Co(II)(CN-Im)Cbl (green). The computed energies and intensities of individual transitions of Co(II)Cbl and Co(II)(F-Im)Cbl are shown as sticks. Details regarding the labeled transitions are provided in Tables 4 and 5

Table 4. TD-DFT Computed Energies, Percent Contributions from Dominant One-Electron Excitations, and Oscillator Strengths for the Major Electronic Transitions of Co(II)Cbl

state	E (cm^{-1})	f	transition	%	donor MO	acceptor MO
1	21 529	0.0666	191b → 193b	45	corrin π/Co 3d$_{z^2}$	corrin π*/Co 3d$_{yz}$
			193a → 194a	19	corrin π /Co 3d$_{z^2}$/ N(DMB)	corrin π*/Co 3d$_{yz}$
2	23 006	0.0235	192a → 194a	14	corrin π/Co 3d$_{yz}$	corrin π*/Co 3d$_{yz}$
			192b → 193b	13	Co 3d$_{yz}$/corrin π	corrin π*/Co 3d$_{yz}$
			191a → 194a	12	Co 3d$_{xz}$/ DMB(π)	corrin π*/Co 3d$_{yz}$
			191b → 194b	11	Corrin π/Co 3d$_{z^2}$	corrin π*/Co 3d$_{xz}$
3	26 202	0.0622	190a → 194a	63	Co 3d$_{z^2}$/N(DMB)/corrin π	corrin π*/Co 3d$_{yz}$
4	28 627	0.0527	192b → 194b	15	Co 3d$_{yz}$/corrin π	corrin π*/Co 3d$_{xz}$
			192a → 195a	12	corrin π/Co 3d$_{yz}$	corrin π*/Co 3d$_{xz}$
			191b → 194b	11	corrin π/Co 3d$_{z^2}$	corrin π*/Co 3d$_{xz}$
5	29 726	0.0217	189b → 193b	32	DMB(π)	corrin π*/Co 3d$_{yz}$
			192b → 195b	11	Co 3d$_{yz}$/corrin π	DMB(π*)
7	36 629	0.2237	191b → 197b	17	corrin π/ Co 3d$_{z^2}$	corrin π*
			190a → 198a	8	Co 3d$_{z^2}$/ N(DMB)/corrin π	corrin π*/Co 3d$_{x^2-y^2}$
			183b → 193b	6	corrin π	corrin π*/Co 3d$_{yz}$
			185b → 193b	6	corrin π	corrin π*/Co 3d$_{yz}$

4. DISCUSSION

The mechanism by which AdoCbl-dependent isomerases accomplish the impressive rate enhancement of homolytic cleavage of the cofactor's Co−C bond has been the subject of intense investigation. Despite extensive research indicating a relative stabilization of the enzyme-bound Co(II)Cbl state, the role of the conserved DXHXGXK motif has not yet been conclusively determined. In the following sections, we discuss the implications of our spectroscopic and computational results with regard to the role that this hydrogen bonding network may play in the mechanism of Co−C bond activation employed by Class I isomerases.

4.1. Axial Ligand Effects on Electronic Structures of Co(III)Cbls. A comparison of the AdoCbl and Ado(F-Im)Cbl spectroscopic and computational results reveals that altering the basicity of the lower axial ligand has relatively minor effects on the electronic structure of the cofactor. Differences observed in the γ region of the Abs spectra can be attributed to different degrees of mixing between the various corrin $\pi \rightarrow \pi$* and CT transitions that contribute to this region. Both our computational analysis and spectroscopic data indicate that the electronic structures of AdoCbl and Ado(F-Im)Cbl are similar but not identical. Most notably, the F-Im frontier orbitals exhibit less mixing with the Co 3d orbitals because of the reduced basicity of the F-Im ligand relative to DMB. The most noticeable impact of this difference on the computed Abs spectra for AdoCbl and Ado(F-Im)Cbl is a redistribution of intensity in the γ region.

4.2. Axial Ligand Effects on Co(II)Cbl and Its Analogues. The most significant differences between the experimental MCD spectra of Co(II)(F-Im)Cbl and Co(II)Cbl occur in the 17 000−20 000 cm^{-1} region, which is dominated by MLCT transitions. In general, the major features in this region of the Co(II)(F-Im)Cbl spectrum are blue-shifted relative to their counterparts in the Co(II)Cbl spectrum. A Gaussian deconvolution of the Abs and MCD spectra reveals that features outside this energy window also undergo blue-shifts in response to lower axial ligand substitution. Similar shifts are predicted for the transitions that dominate the computed Abs spectra. An inspection of the corresponding EDDMs reveals that these transitions have significant MLCT character. A blue-shifting of MLCT transitions can be explained by invoking a stabilization of all Co 3d-based MOs relative to the ligand MOs, which could be accomplished by a reduction in electron donation from the α-axial ligand to the Co(II) ion.

Table 5. TD-DFT Computed Energies, Shifts From Corresponding Co(II)Cbl Transitions, Oscillator Strengths, and Percent Contributions from Dominant One-Electron Excitations for the Major Electronic Transitions of Co(II)(F-Im)Cbl

state	E (cm^{-1})	shift (cm^{-1})	f	transition	%	donor MO	acceptor MO
1	22 191	662	0.1007	174b → 176b	46	corrin π/Co 3d$_{yz}$	corrin π*/Co 3d$_{yz}$
				176a → 177a	25	corrin π/Co 3d$_{z^2}$/N(F-Im)	corrin π*/Co 3d$_{yz}$
2	23 498	492	0.0389	175b → 176b	21	corrin π/Co 3d$_{yz}$	corrin π*/Co 3d$_{yz}$
				175a → 177a	18	corrin π/Co 3d$_{yz}$	corrin π*/Co 3d$_{yz}$
				174b → 177b	13	corrin π/Co 3d$_{yz}$	corrin π*/Co 3d$_{z^2}$
3	26 268	66	0.0352	174a → 177a	47	Co 3 d$_{xz}$/corrin π	corrin π*/Co 3d$_{yz}$
				175a → 178a	24	corrin π/Co 3d$_{yz}$	corrin π*/Co 3d$_{yz}$
4	29 056	429	0.0699	175b → 177b	19	corrin π/Co 3d$_{yz}$	corrin π*/Co 3d$_{z^2}$
				175a → 178a	12	corrin π/Co 3d$_{yz}$	corrin π*/Co 3d$_{xz}$
				174b → 180b	8	corrin π/Co 3d$_{yz}$	corrin π*/F-Im-π*
5	30 272	546	0.0564	176a → 178a	23	corrin π/Co 3d$_{z^2}$/N(F-Im)	corrin π*/Co 3d$_{yz}$
				175b → 180b	13	corrin π/Co 3d$_{yz}$	corrin π*/F-Im-π*
				172a → 177a	13	Co 3d$_{yz}$/corrin π	corrin π*/Co 3d$_{yz}$
6	33 289	N/A	0.0766	173a → 178a	19	Co 3d$_{z^2}$/N(F-Im)	corrin π*/Co 3d$_{xz}$
				169a → 177a	17	Co 3d$_{xy}$/F-Im-π	corrin π*/Co 3d$_{yz}$
				172a → 177a	13	Co 3d$_{yz}$/corrin π	corrin π*/Co 3d$_{yz}$
7	36 588	−41	0.1694	174b → 180b	19	corrin π/Co 3d$_{yz}$	corrin π*/F-Im-π*
				173a → 178a	8	Co 3d$_{z^2}$/N(F-Im)	corrin π*/Co 3d$_{xz}$
				167b → 176b	8	Corrin π	corrin π*/Co 3d$_{yz}$

Transition	1	2	3	4	5
Co(II)Cbl					
Co(II) (F-Im)Cbl					
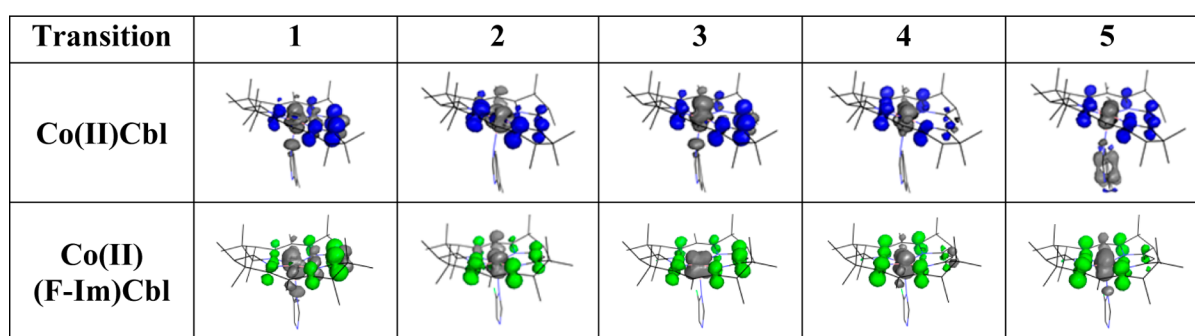
Figure 8. EDDMs for transitions 1−5 in the TD-DFT computed Abs spectra of Co(II)Cbl and Co(II)(F-Im)Cbl in Figure 7. Regions of electron density loss are shown in gray, and regions of electron density gain are shown in blue [Co(II)Cbl] or green [Co(II)(F-Im)Cbl].
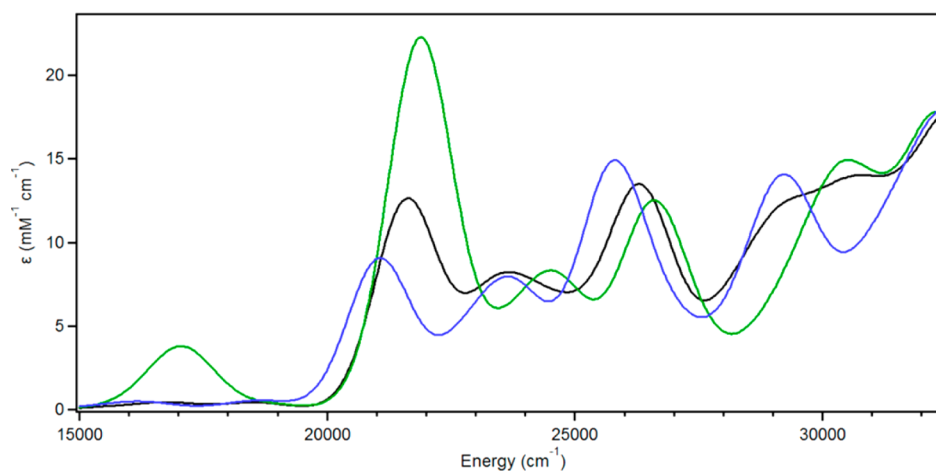
Figure 9. TD-DFT computed Abs spectra for three Co(II)-bound Cbi derivatives: Co(II)pyCbi$^+$ (black), Co(II)(Me$_2$N-py)Cbi$^+$ (blue), and Co(II)(CN-py)Cbi$^+$ (green).

Though other factors may contribute to these blue shifts, our results are consistent with a stabilization of the Co(II) form of the cofactor via replacement of the lower axial ligand with a weaker base. To confirm that the observed spectral changes are indeed due, primarily, to changes in α-axial ligand basicity, we

performed experimental and computational studies of multiple Co(II)Cbl and Co(II)Cbi$^+$ species with variable lower axial ligation. The MCD spectra of the Co(II)Cbi$^+$ derivatives indicate that a decrease in lower axial ligand basicity causes blue shifts of features throughout the spectrum, an observation
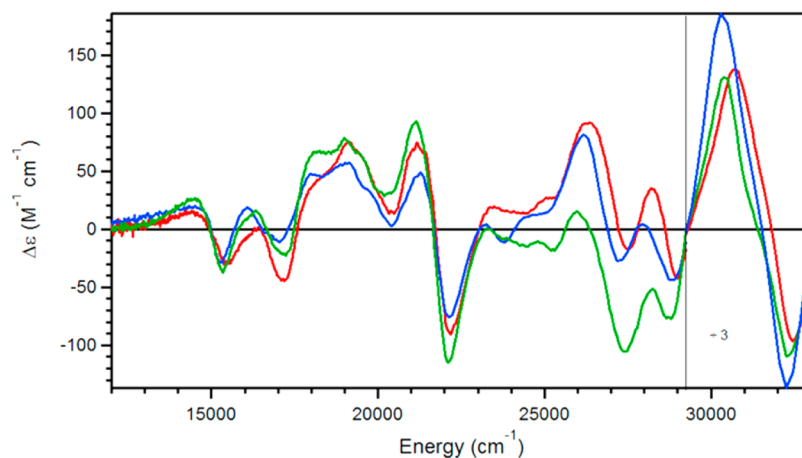
Figure 10. MCD spectra of Co(II)F-Im)Cbl (red), MMCM-bound Co(II)Cbl (green), and GM-bound Co(II)Cbl (blue), obtained at 4.5 K and 7 T.

corroborated by our TD-DFT results. Similarly, the computational study of additional Co(II)Cbl derivatives reveals that MLCT transitions of these species are blue-shifted in the presence of weaker α-axial ligands.

The fact that replacement of the DMB ligand with F-Im induces more noticeable changes to the Abs and MCD spectra of Co(II)Cbl than to those of AdoCbl can be explained in terms of the different relative importance of the axial bonding interactions in these species. In Co(II)Cbl, the singly occupied Co $3d_{z^2}$-based MO is characterized by a strong σ*-antibonding interaction with the coordinating nitrogen of the lower axial ligand. Replacement of the axial ligand with a weaker base results in a large reduction of this antibonding interaction and thus causes a significant stabilization of the Co $3d_{z^2}$-based MO. Alternatively, in AdoCbl, the stabilizing effect of a weaker α-axial ligand is limited because the Co $3d_{z^2}$-based MO also contains a large σ*-antibonding contribution from the strongly σ-donating Ado ligand. Consequently, reducing the basicity of the α-axial ligand results in more modest changes to the cofactor's electronic structure in the Co(III) state. Consistent with these predictions, it has previously been shown that a correlation exists between the Co−C bond dissociation energy and α-axial ligand basicity in cobaloximes, a class of synthetic Cbl model complexes.[48] However, the weakening of the Co−C bond predicted upon replacement of the native DMB ligand with the more weakly donating Im or F-Im bases is far smaller than what is observed in AdoCbl-dependent enzymes, implying that the actual mechanism of Co−C bond activation is more complicated.

4.3. Implications for Co−C Bond Activation by Class I Isomerases. The biological relevance of the Co(II)(F-Im)Cbl cofactor analogue is highlighted by the striking resemblance of its MCD spectrum to those of Co(II)Cbl bound to the Class I isomerases GM and MMCM (Figure 10). Given this similarity, it is likely that the perturbations to the electronic structure of Co(II)Cbl induced by binding to GM and MMCM are analogous to those induced by replacing the lower axial ligand with a weaker base. However, our results indicate that the same ligand switch that causes these changes in the Co(II) form of the free cofactor also induces small changes to the Co(III) form, and that these changes do not mimic those seen upon AdoCbl binding to GM[29] and MMCM.[34] Thus, it appears that the reduced basicity of F-Im makes Co(II)(F-Im)Cbl an

excellent model for enzyme-bound Co(II)Cbl, while Ado(F-Im)Cbl only partially mimics enzyme-bound AdoCbl.

The blue shifts of the MLCT transitions in the MCD spectra of the enzyme-bound versus free Co(II)Cbl cofactor were interpreted previously[28,29] as an indication of a uniform stabilization of the Co 3d orbitals. Class I isomerases like GM and MMCM may facilitate this stabilization through a hydrogen bonding network within the His, Asp, Lys triad of conserved residues. Proton uptake by this triad would reduce the electron-donating power of the coordinating His, resulting in reduced charge donation from the His to the Co ion. Since the spectral perturbations associated with the reduced basicity of this ligand are observed only in the Co(II)Cbl form of the enzyme-bound cofactor, we propose that proton uptake is coupled to Co−C bond homolysis. The preferential stabilization of the posthomolysis Co(II)Cbl product over the AdoCbl form by the enzyme active site is expected to provide a significant contribution to the overall reduction in the barrier to Co−C bond homolysis. Interestingly, this mechanism is only possible in Class I isomerases, because of the unique His-on binding mode employed by these enzymes. Class II eliminases, which bind AdoCbl in the DMB-on form, must lower the barrier to homolysis by another mechanism, given that the native DMB ligand is incapable of hydrogen bonding. Therefore, the reduced catalytic efficiency of Ado(F-Im)Cbl in RNTR is likely caused by factors other than the low basicity of the F-Im ligand. Indeed, preliminary MCD spectroscopic data obtained for AdoCbl and Co(II)Cbl bound to the Class II enzyme ethanolamine ammonia lyase (not shown) are more consistent with a mechanism invoking destabilization of the AdoCbl reactant state, as opposed to stabilization of the Co(II)Cbl posthomolysis product.

Finally, we note that the addition of substrate causes further blue shifts of the MCD features of GM- and MMCM-bound Co(II)Cbl,[28,29] suggesting that an additional decrease in the α-axial ligand basicity occurs in this process. Since the hydrogen bonding network is unlikely to take up another proton, it may be that binding of substrate affects the relative positioning of Co(II)Cbl and/or the position of the proton. That is, the presence of substrate may induce changes to the geometry of the cofactor or the DXHXGXK motif such that the extra proton present in the Co(II)Cbl state becomes more closely associated with the His, which therefore becomes an even weaker base. This mechanism would allow the enzyme to

control the timing of Co—C bond homolysis, ensuring that the highly reactive Ado• radical is formed only when substrate is available to reduce the risk of undesirable side reactions or radical escape into the cell.

5. CONCLUSION

There are many possible ways to account for the $\sim 10^{12}$-fold acceleration of the homolytic Co—C bond cleavage that is achieved by the AdoCbl-dependent Class I isomerases.[81] Increasing evidence exists[20,23,28,29,32,82] indicating that this rate acceleration is due, at least in part, to a stabilization of the posthomolysis Ado• and Co(II)Cbl products within the active site by a combination of favorable electrostatic interactions and electronic effects involving the axial base. We have presented evidence that one factor contributing to the stabilization of the Co(II)Cbl intermediate is a reduction in charge donation from the lower axial ligand to the central Co ion, which results in a fairly uniform stabilization of the Co 3d-based MOs. In the enzyme active site, this stabilization could occur via proton uptake by the catalytic triad, thus explaining the necessity of this conserved motif for the impressive enzymatic acceleration of Co—C bond homolysis by Class I isomerases.

■ ASSOCIATED CONTENT

ⓢ Supporting Information

EPR parameters and spectra of Co(II)Cbi$^+$ derivatives, QM/MM optimized geometries, geometric parameters, fit parameters, Gaussian deconvolutions of the Abs and MCD spectra of Co(II)Cbl and Co(II)(F-Im)Cbl, isosurface plots of relevant frontier MOs, computed MO diagrams, computed Abs spectra, and Cartesian coordinates for all geometry-optimized models discussed in the text. This material is available free of charge via the Internet at http://pubs.acs.org.

■ AUTHOR INFORMATION

Corresponding Author

*E-mail: brunold@chem.wisc.edu. Phone: (608) 265-9056. Fax: (608) 262-6143.

Present Address

⊥Dept. of Structural Biology and Biophysics, Worldwide Research and Development, Pfizer, Inc., Groton, CT 06340.

Notes

The authors declare no competing financial interest.

■ ACKNOWLEDGMENTS

■ REFERENCES

(1) Banerjee, R. *Chem. Rev.* **2003**, *103*, 2083.
(2) Toraya, T. *Arch. Biochem. Biophys.* **2014**, *544*, 40.
(3) Marsh, E. N. G.; Melendez, G. D. R. *Biochim. Biophys. Acta, Proteins Proteomics* **2012**, *1824*, 1154.
(4) Brown, K. L. *Chem. Rev.* **2005**, *105*, 2075.
(5) Roth, J. R.; Lawrence, J. G.; Bobik, T. A. *Annu. Rev. Microbiol.* **1996**, *50*, 137.
(6) Kolhouse, J. F.; Allen, R. H. *Proc. Natl. Acad. Sci. U. S. A.* **1977**, *74*, 921.
(7) Chowdhury, S.; Banerjee, R. *Biochemistry* **2000**, *39*, 7998.
(8) Marsh, E. N. G.; Ballou, D. P. *Biochemistry* **1998**, *37*, 11864.
(9) Marsh, E. N. G.; Holloway, D. E. *FEBS Lett.* **1992**, *310*, 167.
(10) Ratnatilleke, A.; Vrijbloed, J. W.; Robinson, J. A. *J. Biol. Chem.* **1999**, *274*, 31679.
(11) Beatrix, B.; Zelder, O.; Linder, D.; Buckel, W. *Eur. J. Biochem.* **1994**, *221*, 101.
(12) Toraya, T. *Chem. Rev.* **2003**, *103*, 2095.
(13) Poppe, L.; Stupperich, E.; Hull, W. E.; Buckel, T.; Retey, J. *Eur. J. Biochem.* **1997**, *250*, 303.
(14) Poppe, L.; Bothe, H.; Broker, G.; Buckel, W.; Stupperich, E.; Retey, J. *J. Mol. Catal. B: Enzym.* **2000**, *10*, 345.
(15) Chowdhury, S.; Thomas, M. G.; Escalante-Semerena, J. C.; Banerjee, R. *J. Biol. Chem.* **2001**, *276*, 1015.
(16) Pierik, A. J.; Ciceri, D.; Lopez, R. F.; Kroll, F.; Broker, G.; Beatrix, B.; Buckel, W.; Golding, B. T. *Biochemistry* **2005**, *44*, 10541.
(17) Chen, H. P.; Marsh, E. N. G. *Biochemistry* **1997**, *36*, 7884.
(18) Vlasie, M.; Chowdhury, S.; Banerjee, R. *J. Biol. Chem.* **2002**, *277*, 18523.
(19) Vlasie, M. D.; Banerjee, R. *J. Am. Chem. Soc.* **2003**, *125*, 5431.
(20) Makins, C.; Pickering, A. V.; Mariani, C.; Wolthers, K. R. *Biochemistry* **2013**, *52*, 878.
(21) Madhavapeddi, P.; Marsh, E. N. G. *Chem. Biol.* **2001**, *8*, 1143.
(22) Xia, L.; Ballou, D. P.; Marsh, E. N. G. *Biochemistry* **2004**, *43*, 3238.
(23) Roman-Melendez, G. D.; von Glehn, P.; Harvey, J. N.; Mulholland, A. J.; Marsh, E. N. G. *Biochemistry* **2014**, *53*, 169.
(24) Weigl, U.; Heimberger, M.; Pierik, A. L.; Retey, J. *Chem.—Eur. J.* **2003**, *9*, 652.
(25) Ng, F. T. T.; Rempel, G. L.; Halpern, J. *Inorg. Chim. Acta* **1983**, *77*, L165.
(26) Halpern, J. *Science* **1985**, *227*, 869.
(27) Sharma, P. K.; Chu, Z. T.; Olsson, M. H. M.; Warshel, A. *Proc. Natl. Acad. Sci. U. S. A.* **2007**, *104*, 9661.
(28) Brooks, A. J.; Vlasie, M.; Banerjee, R.; Brunold, T. C. *J. Am. Chem. Soc.* **2005**, *127*, 16522.
(29) Brooks, A. J.; Fox, C. C.; Marsh, E. N. G.; Vlasie, M.; Banerjee, R.; Brunold, T. C. *Biochemistry* **2005**, *44*, 15167.
(30) Durbeej, B.; Sandala, G. M.; Bucher, D.; Smith, D. M.; Radom, L. *Chem.—Eur. J.* **2009**, *15*, 8578.
(31) Dolker, N.; Maseras, F.; Siegbahn, P. E. M. *Chem. Phys. Lett.* **2004**, *386*, 174.
(32) Friedrich, P.; Baisch, U.; Harrington, R. W.; Lyatuu, F.; Zhou, K.; Zelder, F.; McFarlane, W.; Buckel, W.; Golding, B. T. *Chem.—Eur. J.* **2012**, *18*, 16114.
(33) Li, X.; Chung, L. W.; Paneth, P.; Morokuma, K. *J. Am. Chem. Soc.* **2009**, *131*, 5115.
(34) Brooks, A. J.; Vlasie, M.; Banerjee, R. V.; Brunold, T. C. *J. Am. Chem. Soc.* **2004**, *126*, 8167.
(35) Ludwig, M. L.; Matthews, R. G. *Annu. Rev. Biochem.* **1997**, *66*, 269.
(36) Pratt, J. M. *J. Inorg. Biochem.* **1986**, *28*, 145.
(37) Pratt, J. M. *Chem. Soc. Rev.* **1985**, *14*, 161.
(38) Brown, K. L. *Dalton Trans.* **2006**, 1123.
(39) Yeh, H. J. C.; Kirk, K. L.; Cohen, L. A.; Cohen, J. S. *J. Chem. Soc., Perkin Trans. 2* **1975**, 928.
(40) Marques, H. M.; Egan, T. J.; Marsh, J. H.; Mellor, J. R.; Munro, O. Q. *Inorg. Chim. Acta* **1989**, *166*, 249.
(41) Note that, while fluoro substituents have nuanced effects on the reactivity of aromatic compounds because of competing inductive and resonance effects, in this work we used F-Im primarily because of its reduced basicity that results from the substituent's electron withdrawing power
(42) Kozlowski, P. M.; Zgierski, M. Z. *J. Phys. Chem. B* **2004**, *108*, 14163.
(43) Mancia, F.; Keep, N. H.; Nakagawa, A.; Leadlay, P. F.; McSweeney, S.; Rasmussen, B.; Bosecke, P.; Diat, O.; Evans, P. R. *Structure* **1996**, *4*, 339.
(44) Scheuring, E.; Padmakumar, R.; Banerjee, R.; Chance, M. R. *J. Am. Chem. Soc.* **1997**, *119*, 12192.

(45) Jensen, K. P.; Ryde, U. *J. Mol. Struct.: THEOCHEM* **2002**, *585*, 239.

(46) Andruniow, T.; Kuta, J.; Zgierski, M. Z.; Kozlowski, P. M. *Chem. Phys. Lett.* **2005**, *410*, 410.

(47) Kuta, J.; Wuerges, J.; Randaccio, L.; Kozlowski, P. M. *J. Phys. Chem. A* **2009**, *113*, 11604.

(48) De March, M.; Demitri, N.; Geremia, S.; Hickey, N.; Randaccio, L. *J. Inorg. Biochem.* **2012**, *116*, 215.

(49) Govender, P. P.; Navizet, I.; Perry, C. B.; Marques, H. M. *J. Phys. Chem. A* **2013**, *117*, 3057.

(50) Sirovatka, J. M.; Finke, R. G. *Inorg. Chem.* **1999**, *38*, 1697.

(51) Dong, S.; Padmakumar, R.; Banerjee, R.; Spiro, T. G. *J. Am. Chem. Soc.* **1996**, *118*, 9182.

(52) Puckett, J.; J. M; Mitchell, M. B.; Hirota, S.; Marzilli, L. G. *Inorg. Chem.* **1996**, *35*, 4656.

(53) Horig, J. A.; Renz, P.; Heckmann, G. *J. Biol. Chem.* **1978**, *253*, 7410.

(54) Kraeutler, B.; Konrat, R.; Stupperich, E.; Faerber, G.; Gruber, K.; Kratky, C. *Inorg. Chem.* **1994**, *33*, 4128.

(55) Stupperich, E.; Steiner, I.; Ruhlemann, M. *Anal. Biochem.* **1986**, *155*, 365.

(56) Renz, P.; Donald, B. M.; Lemuel, D. W. *Methods Enzymol.* **1971**, *18* (Part C), 82.

(57) Park, K.; Mera, P. E.; Escalante-Semerena, J. C.; Brunold, T. C. *Biochemistry* **2008**, *47*, 9007.

(58) Stich, T. A.; Buan, N. R.; Escalante-Semerena, J. C.; Brunold, T. C. *J. Am. Chem. Soc.* **2005**, *127*, 8710.

(59) Harmer, J.; Van Doorslaer, S.; Gromov, I.; Schweiger, A. *Chem. Phys. Lett.* **2002**, *358*, 8.

(60) Neese, F. Electronic Structure and Spectroscopy of Novel Copper Chromophores in Biology. Ph.D. Thesis, University of Konstanz, 1997.

(61) Lenhert, P. G. *Proc. R. Soc. London, Ser. A* **1968**, *303*, 45.

(62) Vreven, T.; Byun, K. S.; Komaromi, I.; Dapprich, S.; Montgomery, J. A.; Morokuma, K.; Frisch, M. J. *J. Chem. Theory Comput.* **2006**, *2*, 815.

(63) Frisch, M. J.; Trucks, G. W.; Schlegel, H. B.; Scuseria, G. E.; Robb, M. A.; Cheeseman, J. R.; Scalmani, G.; Barone, V.; Mennucci, B.; Petersson, G. A.; Nakatsuji, H.; Caricato, M.; Li, X.; Hratchian, H. P.; Izmaylov, A. F.; Bloino, J.; Zheng, G.; Sonnenberg, J. L.; Hada, M.; Ehara, M.; Toyota, K.; Fukuda, R.; Hasegawa, J.; Ishida, M.; Nakajima, T.; Honda, Y.; Kitao, O.; Nakai, H.; Vreven, J. A.; Montgomery, J. A.; Peralta, J. E.; Ogliaro, F.; Bearpark, M.; Heyd, J. J.; Brothers, E.; Kudin, K. N.; Staroverov, V. N.; Kobayashi, R.; Normand, J.; Raghavachari, K.; Rendell, A.; Burant, J. C.; Iyengar, S. S.; Tomasi, J.; Cossi, M.; Rega, N.; Millam, J. M.; Klene, M.; Knox, J. E.; Cross, J. B.; Bakken, V.; Adamo, C.; Jaramillo, J.; Gomperts, R.; Stratmann, R. E.; Yazyev, O.; Austin, A. J.; Cammi, R.; Pomelli, C.; Ochterski, J. W.; Martin, R. L.; Morokuma, K.; Zakrzewski, V. G.; Voth, G. A.; Salvador, P.; Danneberg, J. J.; Dapprich, S.; Daniels, A. D.; Farkas, O.; Foresman, J. B.; Ortiz, J. V.; Cioslowski, J.; Fox, D. G. *Gaussian 09*; Revision D.01; Gaussian Inc.: Wallingford, CT, 2009.

(64) Becke, A. D. *J. Chem. Phys.* **1993**, *98*, 1372.

(65) Perdew, J. P. *Phys. Rev. B: Condens. Matter Mater. Phys.* **1986**, *33*, 8822.

(66) Kuta, J.; Patchkovskii, S.; Zgierski, M. Z.; Kozlowski, P. M. *J. Comput. Chem.* **2006**, *27*, 1429.

(67) Schafer, A.; Huber, C.; Ahlrichs, R. *J. Chem. Phys.* **1994**, *100*, 5829.

(68) Schafer, A.; Horn, H.; Ahlrichs, R. *J. Chem. Phys.* **1992**, *97*, 2571.

(69) Marques, H. M.; Ngoma, B.; Egan, T. J.; Brown, K. L. *J. Mol. Struct.* **2001**, *561*, 71.

(70) Lee, C. T.; Yang, W. T.; Parr, R. G. *Phys. Rev. B: Condens. Matter Mater. Phys.* **1988**, *37*, 785.

(71) Stich, T. A.; Buan, N. R.; Brunold, T. C. *J. Am. Chem. Soc.* **2004**, *126*, 9735.

(72) Stich, T. A.; Brooks, A. J.; Buan, N. R.; Brunold, T. C. *J. Am. Chem. Soc.* **2003**, *125*, 5897.

(73) Kornobis, K.; Kumar, N.; Lodowski, P.; Jaworska, M.; Piecuch, P.; Lutz, J. J.; Wong, B. M.; Kozlowski, P. M. *J. Comput. Chem.* **2013**, *34*, 987.

(74) Tao, J. M.; Perdew, J. P.; Staroverov, V. N.; Scuseria, G. E. *Phys. Rev. Lett.* **2003**, *91*, 4.

(75) Neese, F. *Wiley Interdiscip. Rev.: Comput. Mol. Sci.* **2012**, *2*, 73.

(76) Neese, F.; Olbrich, G. *Chem. Phys. Lett.* **2002**, *362*, 170.

(77) Hirata, S.; Head-Gordon, M. *Chem. Phys. Lett.* **1999**, *314*, 291.

(78) The PyMOL Molecular Graphics System, Version 1.5.0.4 Schrodinger, LLC. Online: https://www.pymol.org/.

(79) Reig, A. J.; Conrad, K. S.; Brunold, T. C. *Inorg. Chem.* **2012**, *51*, 2867.

(80) Hofmann, K. *Imidazole and its derivatives*; Interscience Publishers: New York, NY, 1953; Vol. 6.

(81) Jensen, K. P.; Ryde, U. *J. Am. Chem. Soc.* **2005**, *127*, 9117.

(82) Buckel, W.; Friedrich, P.; Golding, B. T. *Angew. Chem., Int. Ed.* **2012**, *51*, 9974.